

Magnetic phase diagram in the Co-rich side of $\text{LnCo}_{1-x}\text{Fe}_x\text{AsO}$ ($\text{Ln}=\text{La}, \text{Sm}$) system

Y. K. Li^{1,2}, X. F. Xu¹, C. Cao¹, C. Y. Shen², Y. K. Luo², Q. Tao², X. Lin¹, L. Zhang³, G. H. Cao² and Z. A. Xu²

¹*Department of Physics, Hangzhou Normal University, Hangzhou 310036, China*

²*State Key Lab of Silicon Materials and Department of Physics, Zhejiang University, Hangzhou 310027, China*

³*Department of Physics, China Jiliang University, Hangzhou 310018, China*

(Dated: November 8, 2018)

The magnetic phase diagram has been mapped out via the measurements of electronic resistivity, magnetization and specific heat in the cobalt-based layered $\text{LnCo}_{1-x}\text{Fe}_x\text{AsO}$ ($\text{Ln}=\text{La}, \text{Sm}$) compounds. The ferromagnetic (FM) transition at ~ 63 K for LaCoAsO is rapidly suppressed upon Fe doping, and ultimately disappears around $x = 0.3$ in the $\text{LaCo}_{1-x}\text{Fe}_x\text{AsO}$ system. When La is replaced by magnetic rare earth element Sm, the 3d-electrons first undergo a FM transition at $T_c \sim 75$ K, followed by an antiferromagnetic (AFM) transition at a lower temperature $T_{N1} \sim 45$ K. With partial Fe doping on the Co site, both FM (T_c) and AFM (T_{N1}) transition temperatures are significantly suppressed, and finally approach zero kelvin at $x = 0.3$ and 0.2, respectively. Meanwhile, a third magnetic transition at $T_{N2} \sim 5.6$ K for SmCoAsO , associated with the AFM order of the Sm^{3+} 4f-moments, is uncovered and T_{N2} is found to be almost robust against the small Fe-doping. These results suggest that the 4f-electrons of Sm^{3+} have an important effect on the magnetic behavior of 3d electrons in the 1111 type Co-based $\text{LnCo}_{1-x}\text{Fe}_x\text{AsO}$ systems. In contrast, the magnetism of the f-electrons is relatively unaffected by the variation of the 3d electrons. The rich magnetic phase diagram in the Co-rich side of the $\text{LnCo}_{1-x}\text{Fe}_x\text{AsO}$ system, therefore, is established.

PACS numbers: 75.30.Kz; 74.25.Dw

I. INTRODUCTION

Correlated electron systems LnTmPnO [$\text{Ln}=\text{rare earth element}$, $\text{Tm}=\text{transition metal element}$, $\text{Pn}=\text{pnictogen element}$] have attracted great attention due to their various electronic and magnetic properties, such as high transition temperature superconductivity¹, itinerant ferromagnetism^{2,3}, giant magnetoresistance⁴, spin density wave (SDW)⁵ and structural instability⁶. For example, iso-structural LaOMnAs is an AFM semiconductor⁷, and LaONiAs shows superconductivity below 3 K⁸. In the case of $\text{Tm}=\text{Co}$, LnCoAsO was reported to be an itinerant ferromagnet with the Curie temperature T_c between 60 and 80 K for La and Sm, respectively^{2,9}. Among them, the compound LaFeAsO , which is a parent compound of well-known iron-based superconductors, exhibits a spin-density wave antiferromagnetic transition at about 150 K¹. When Fe is partially replaced by Co atoms, the AFM order from Fe ions is suppressed and then superconductivity emerges, and the compound exhibits a good metallic behavior down to superconducting (SC) transition temperature^{10,11}. Similar results have also been reported for Co-doped CeFeAsO ¹², PrFeAsO ^{13,14}, NdFeAsO ¹⁵ and SmFeAsO ¹¹ systems. Thus, magnetism is closely related to superconductivity in these iron-based high-temperature superconductors.

On the other hand, the LnCoAsO compounds (also referred to as Co-1111 system) with the same space group as ZrCuSiAs exhibit rich magnetic properties at low temperature. LaCoAsO is reported to be an itinerant ferromagnet with 2D ferromagnetic spin fluctuations^{2,16}. When La is substituted by other magnetic rare earth elements, LnCoAsO ($\text{Ln}=\text{Nd}, \text{Sm}, \text{and Gd}$)^{9,17-21} under-

goes multiple magnetic phase transitions as the temperature decreases. Furthermore, the AFM order due to the magnetic sublattice of Ln ions at very low temperature can be also observed in those compounds, almost irrelevant to the doping at Tm or Pn sites. For example, in the case of SmCoAsO ²⁰, a ferromagnetic (FM) transition occurs around T_c of 75 K, followed by a FM-AFM transition from the magnetic coupling between the CoAs layers around 45 K, and finally another AFM order from Sm ion forms at 5.6 K recently reported by other groups^{18,22,23}. Indeed, several groups^{9,25} have suggested that the Ruderman-Kittel-Kasuya-Yoshida (RKKY) interaction may play a role in the FM-AFM transition. It is ascribed to the interaction between the localized magnetic moments of lanthanide 4f electrons and the ferromagnetic ordered magnetic moments of cobalt 3d itinerant electrons. The neutron diffraction experiments^{15,17} and specific heat measurements^{18,22,23} have detected the localized magnetic moment of Ln 4f electrons in those parent compounds.

Up to now, main studies about Co-containing 1111 system focus on these low Co concentrations¹⁰⁻¹⁵ and LnCoPnO parent compounds^{2,4,9,17-20}. There are few reports on the study of chemical doping in LnCoAsO ²⁷, and the magnetic phase diagram on the Co-rich side of LnCoAsO is less known. In this paper, we report our detailed study of the magnetic properties of Fe-doped $\text{LnCo}_{1-x}\text{Fe}_x\text{AsO}$ ($\text{Ln}=\text{La}, \text{Sm}$) system on the Co-rich side. In order to study the interplay between 4f electrons and 3d electrons, $\text{LaCo}_{1-x}\text{Fe}_x\text{AsO}$ system is employed as a comparison. We performed powder X-ray diffraction, electrical resistivity, and magnetization measurements, as well as the first-principles calculations. The results of these measurements and calculations indicate that, the FM order is quickly suppressed by Fe doping in

LaCo_{1-x}Fe_xAsO system, and finally disappears at about $x = 0.3$. In the case of SmCo_{1-x}Fe_xAsO, the FM and AFM transitions of the 3d-electrons are gradually suppressed and then disappear at $x = 0.3$ and 0.2, respectively. However, the AFM order at low temperature due to Sm³⁺ is robust and T_{N2} slightly varies with increasing Fe content. A rich magnetic phase diagram for $x \leq 0.3$ LnCo_{1-x}Fe_xAsO system is therefore established.

II. EXPERIMENTAL

The polycrystalline samples of LnCo_{1-x}Fe_xAsO ($Ln=La, Sm$) were synthesized by two-step solid state reaction methods in vacuum, similar to our previous reports¹¹. The pellets of LnCo_{1-x}Fe_xAsO ($x = 0, 0.05, 0.1, 0.2, 0.3,$) were annealed in an evacuated quartz tube at 1423 K for 40 hours and furnace-cooled to room temperature.

Crystal structure measurement was performed by powder X-ray diffraction (XRD) at room temperature using a D/Max-rA diffractometer with Cu K_α radiation and a graphite monochromator. Lattice parameters were calculated by least-squares fitting using at least 20 XRD peaks. The electrical resistivity was measured by four-terminal method. The temperature dependence of d.c. magnetization was measured on a Quantum Design Magnetic Property Measurement System (MPMS-5). The measurement of specific heat was performed on a Quantum Design Physical Property Measurement System (PPMS-9).

The magnetic properties of LaCo_{1-x}Fe_xAs were calculated using planewave basis pseudopotential method implemented in Quantum *Espresso* package. The exchange-correlation interactions were modeled with Perdew, Burke and Enzerhoff flavor of generalized gradient approximation²⁶. To model the dilute substitutional iron doping effect, a virtual crystal approximation (VCA) was employed to treat Fe/Co sites.

III. RESULTS AND DISCUSSION

A. Magnetic properties in LaCo_{1-x}Fe_xAsO

Fig. 1(a) shows the powder XRD patterns of the typical LaCo_{1-x}Fe_xAsO samples and Fig. 1(b) shows the variations of lattice parameters with respect to the Fe content (x). Where the main diffraction peaks of those samples can be well indexed based on a tetragonal cell of ZrCuSiAs-type structure, weak peaks exist due to impurity phase CoAs. The content of impurity phase CoAs estimated by Rietveld fitting is less than 5%. It is worth noting that CoAs has been reported to be non-magnetic from 4.2 to 300 K². The a -axis decreases slightly with increasing Fe content, and the c -axis increases accordingly, resulting in the increase of the cell volume, since the ionic radius of tetrahedrally coordinated Fe²⁺ ions are larger than that of Co²⁺. The systematic increase in

the c -axis indicates successful substitution of Co by Fe. Similar variations of lattice constants were also observed in the NdFe_{1-x}Co_xAsO in previous reports²⁷.

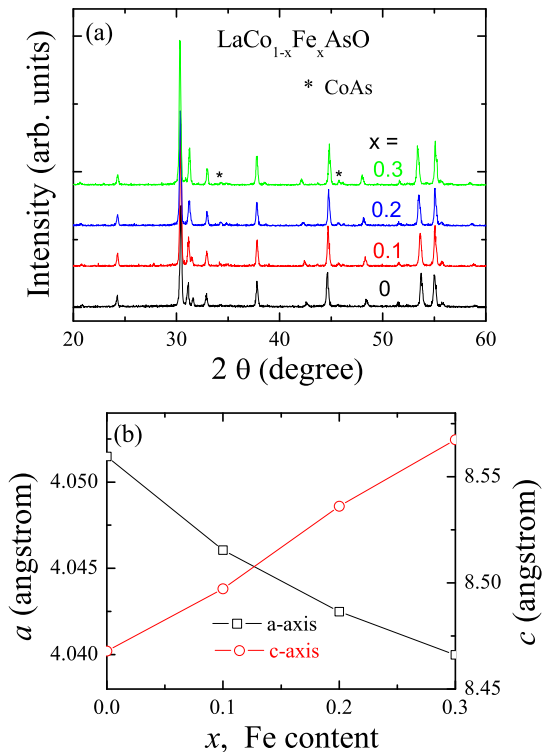


FIG. 1. Structural characterization of LaCo_{1-x}Fe_xAsO samples. (a) Powder X-ray diffraction patterns of representative LaCo_{1-x}Fe_xAsO samples. The asterisked peak positions designate the impurity phase of CoAs. (b) Lattice parameters as functions of Fe content.

Fig. 2 shows the temperature dependence of the electric resistivity (ρ) and magnetic susceptibility (χ) of LaCo_{1-x}Fe_xAsO samples. The inset shows magnetic susceptibility vs. temperature between 100 to 300 K. In Fig. 2(a), for LaCoAsO, the resistivity falls monotonically with decreasing temperature from 300 K, a resistivity hump can be clearly identified at about 63 K, which is related with FM transition temperature T_c . As Fe content increases to 0.1, this hump shifts to about 35 K, and then for $x = 0.2$, the anomaly in resistive is not observed. Actually, the anomaly around T_c becomes more obvious in the derivative of ρ shown in Fig. 2(b), where T_c decreases with increasing Fe content and shifts to below 2 K at $x = 0.3$. Meanwhile, the resistivity value gradually increases with the Fe doping levels, which can be attributed to the less itinerant nature of Fe 3d electron than that of Co. The magnetic susceptibility for the LaCo_{1-x}Fe_xAsO under $H = 1$ kOe in zero field cooled (ZFC) configuration was plotted in Fig. 2(c). For the parent LaCoAsO sample, the magnetic susceptibil-

ity increases dramatically below T_c of 63 K, suggesting that the Co sublattice forms FM order in the CoAs layer. The similar magnetic behavior has been reported in the literature². As Co is partially replaced by Fe, FM transition temperature (T_c) is sharply suppressed and shifts to lower temperature. For $x = 0.3$, the formation of long range FM order cannot be identified in $\chi(T)$ down to 2 K. Furthermore, the magnetic susceptibility value drops to several orders of magnitude of LaCoAsO. On the other hand, it can be seen from inset that the magnetic susceptibility curve above 100 K exhibits the Curie-Weiss behaviors for LaCoAsO. As Fe content increases, the susceptibility gradually becomes less T -dependence and final remains constant for $x = 0.3$, indicating that Fe doping strongly reduces the moment of 3d-electrons in Co-based 1111 compounds.

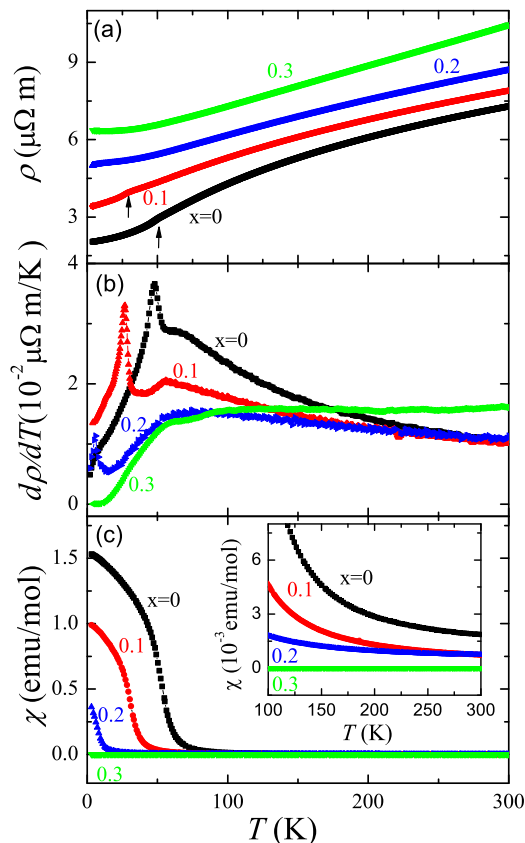


FIG. 2. (a) Temperature dependence of resistivity (ρ) for the $\text{LaCo}_{1-x}\text{Fe}_x\text{AsO}$ ($x = 0, 0.1, 0.2, 0.3$) samples. (b) The derivative of resistivity near the ferromagnetic phase transition. (c) Temperature dependence of magnetic susceptibility (χ) under a magnetic field of 1000 Oe in the zero-field-cooled (ZFC) configuration.

Fig. 3 shows the M-H loop curves at several temperatures for $\text{LaCo}_{1-x}\text{Fe}_x\text{AsO}$. For $x \leq 0.2$, the M-H curves are nearly linear above T_c , indicating that those

compounds are paramagnetic at these temperatures. Below T_c , these curves deviate from linearity and become slightly S-shaped, suggesting the emergence of FM order. Further decreasing temperature to 3 K, the molar magnetization sharply increases and then saturates with the increase of magnetic field, and the small finite hysteresis can be distinguished (the data is not shown here). These results suggest that the ground state of these samples is FM. For $x = 0.3$, the M-H curve always shows the linear behaviors above 3 K, indicating that this sample remains paramagnetic. The magnetic moment M_{s0} estimated by extrapolating the Ms-H curves to $T = 0$ K are $0.35 \mu_B$ per Co for LaCoAsO, which is very close to the value reported previously². With increasing Fe content, M_{s0} quickly decreases, consistent with the fact that the FM transition temperature T_c shifts to lower temperature.

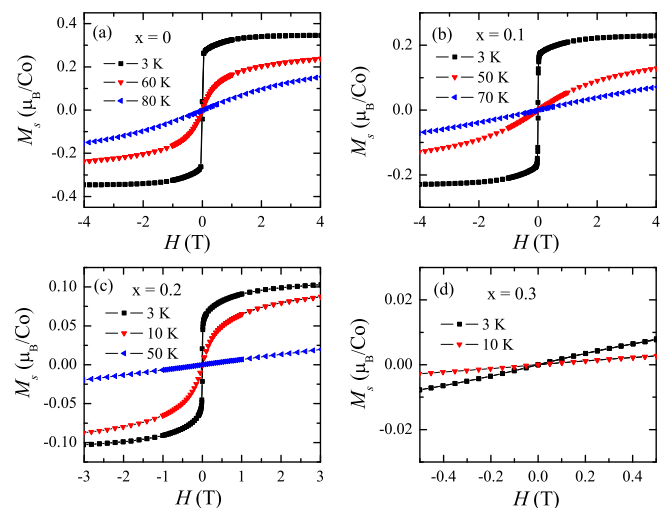


FIG. 3. Field dependence of magnetization at various temperatures for the $\text{LaCo}_{1-x}\text{Fe}_x\text{AsO}$ ($x = 0, 0.1, 0.2, 0.3$) samples.

Fig. 4 shows the LDA calculation results of $\text{LaCo}_{1-x}\text{Fe}_x\text{As}$ system. The ground state of the system were determined by comparing the total energy of three possible long range magnetic orderings, i.e., ferromagnetic (FM), checkerboard antiferromagnetic (CB-AFM) and stripe-like antiferromagnetic (SDW-AFM), as well as the non-magnetic (NM) configurations. As shown in Fig. 4(a), the ground state is clearly FM at the cobalt side ($x=0.0$), where the CB-AFM order cannot be stabilized over the whole range we considered ($0.0 \leq x \leq 0.5$). As x increases, the energy of FM configuration quickly rises, suggesting the iron doping will suppress the formation of FM long-range order. At $x \sim 0.25$, the SDW-AFM order takes over and becomes the ground state. However, one should keep in mind that the disorder effect is not fully taken care of in VCA, and a disordered dopant pattern is detrimental to the formation of AFM long-range

order. Furthermore, the magnetic coupling strength is suppressed with increasing x from $x = 0.2$ to 0.5 , as suggested by increasing configuration energy of both FM and SDW-AFM orders. With these considerations, we conclude that the actual ground state should be paramagnetic with local magnetic fluctuations.

We then compare the LDA lattice structure variation in Fig. 4(b). As the experimental measurements were performed at room temperature when the long range magnetic order was not yet formed, we compare the NM lattice constants. It could be seen that between $x \in [0.0, 0.3]$, the LDA lattice constants show the same trend as the experimental results but with much larger variation. Beyond $x = 0.3$, the lattice constants show much less variation. For the FM phase of $\text{LaCo}_{1-x}\text{Fe}_x\text{AsO}$, we also examine its magnetic moment per transition metal m_{TM} and the arsenic height z_{As} (Fig. 4(c)). At $x = 0.0$, the LaOCoAs compound has a small moment of $0.6 \mu_{\text{B}}/\text{Co}$, indicating weak FM ground state with low Curie temperature. As the doping level x increases, the moment almost linearly decreases to $x = 0.3 \mu_{\text{B}}/\text{TM}$ at $x = 0.3$ at the VCA level. As discussed above, the disorder effect will further suppress the moment. Meanwhile, z_{As} also increases almost linearly with respect to x from $\sim 1.18\text{\AA}$ to $\sim 1.24\text{\AA}$. The variation of z_{As} is consistent with the change of the super-exchange via arsenic, which becomes less FM and more AFM with increasing x .

B. Magnetic properties in $\text{SmCo}_{1-x}\text{Fe}_x\text{AsO}$

Fig. 5(a) shows the powder XRD patterns of $\text{SmCo}_{1-x}\text{Fe}_x\text{AsO}$ samples and Fig. 5(b) shows the variations of lattice parameters with Fe content (x). All those samples are single phase since no extra peak is observed. Similar to the case of $\text{LaCo}_{1-x}\text{Fe}_x\text{AsO}$, Fe doping causes slight decrease in the a -axis, while the c -axis monotonously increases.

Fig. 6 shows the temperature dependence of the electric resistivity and magnetic susceptibility of the $\text{SmCo}_{1-x}\text{Fe}_x\text{AsO}$ samples. In Fig. 6(a), for the undoped parent compound SmCoAsO ²⁰, the resistivity monotonically decreases with decreasing temperature from 300 K, followed by a distinguishable kink around 45 K which can be associated with the FM-AFM transition temperature (defined as T_{N1}). As Fe content increases to 0.1, this kink becomes more pronounced and moves to lower temperatures, and no anomaly is observed below T_{N1} . For $x = 0.2$, the resistivity anomaly related with T_{N1} disappears, but another tiny kink can be identified around 5.1 K, which can be attributed to the AFM transition (T_{N2}) due to the magnetic sublattice of Sm ions. As x increases to 0.3, T_{N2} in the resistivity becomes more remarkable (shown in inset of Fig. 6(a)). In order to identify the magnetic ordering transition more clearly, the derivative of resistivity below 150 K is plotted in Fig. 6 (b), which shows a maximum around T_c , a minimum near T_{N1} , and a peak at T_{N2} . With increasing Fe content, the max-

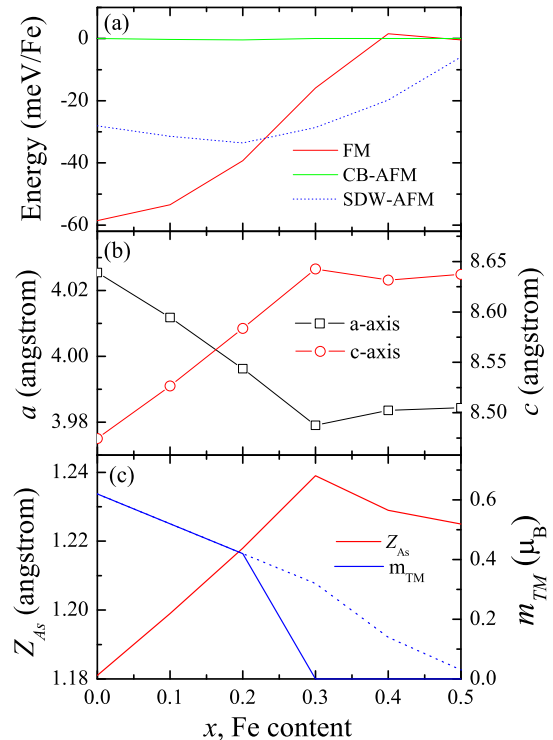


FIG. 4. LDA results of $\text{LaOCo}_{1-x}\text{Fe}_x\text{As}$ properties. a) Magnetic configuration energy (per Fe atom) with respect to NM total energy. b) NM lattice constants variation with respect to x . c) Arsenic height z_{As} and transition metal magnetic moment m_{TM} , the dashed blue line is the actual LDA results for FM phases, while the solid blue line suggests the actual scenario with phase transition taken into consideration.

imum around T_c shifts to lower temperatures, and the minimum near T_{N1} even becomes more pronounced for $x = 0.1$ and disappears as $x = 0.2$. The magnetic susceptibility data is shown in Fig. 6(c), it can be seen that SmCoAsO shows a sharp peak around 45 K. This peak is ascribed to FM to AFM transition of the cobalt sublattice, which has been reported for $Ln = \text{Nd, Sm, and Gd}$ ⁹. As Fe substitutes Co, T_{N1} is gradually suppressed and shifts to lower temperatures. Meanwhile, the intensity of the peaks becomes weaker, consistent with the resistivity data. At $x = 0.2$, it is noted that a tiny hump around 6.5 K is observed, which may not be explained by the AFM transition T_{N1} according to our M-H data (see fig.8). The detailed discussion is beyond the scope of the current work and will be given in the future. When x increases to 0.3, the magnetization sharply drops and a tiny peak is detected at 5.5 K. Considering the specific heat data in Fig. 7, this transition (T_{N2}) is attributed to the AFM ordering of Sm^{3+} sublattice²²⁻²⁴. Similar results can be found in the previous papers^{15,17,24}. For $x < 0.3$ samples, such low temperature peak in mag-

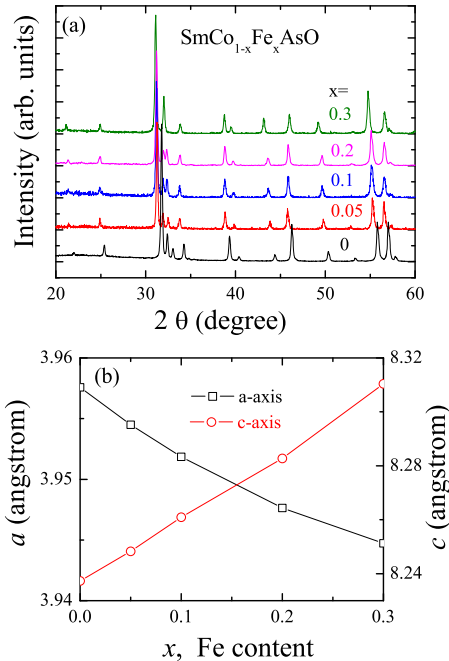


FIG. 5. Structural characterization of $\text{SmCo}_{1-x}\text{Fe}_x\text{AsO}$ samples. (a) Powder X-ray diffraction patterns of representative $\text{SmCo}_{1-x}\text{Fe}_x\text{AsO}$ samples. (b) Lattice parameters as functions of Fe content.

netization curves is not observable due to the magnetic ordering of 3d-electrons.

In order to further study the magnetic phase transition, the zero field specific heat versus temperature curves for those samples are summarized in Fig. 7. For all the samples, no anomaly in the curves is found around T_c associated with the FM transition, which is also the case in NdCoAsO^{17} . A small broad peak related to the AFM transition T_{N1} can be observed at 45 K for SmCoAsO and then shifts to 22 K for $x = 0.1$ (The data is not shown here). However, it is worth noticing that another clear broad peak from the AFM ordering of Sm^{3+} sublattice can be observed at 5.5 K and 3.5 K, respectively. As x increases to 0.2, no extra peak is detected except for the large anomaly near T_{N2} of 5 K, which then shifts to 5.5 K for $x = 0.3$, consistent with the magnetic susceptibility data shown in Fig. 6(c). Similar results are observed in the case of SmFeAsO^{24} , SmCoAsO^{18} and SmCoPO^{23} . However, the hump in SmCoAsO related to the Sm AFM ordering becomes sharper and higher with increasing Fe content, which suggests that the increase of c lattice weakens the coupling of 3d electron and 4f electron. Low temperature specific heat measurements also confirms that the peak associated with T_{N2} is robust as $x \leq 0.3$.

Fig. 8 shows the field dependence of the magnetization at various temperatures for all the samples. As reported

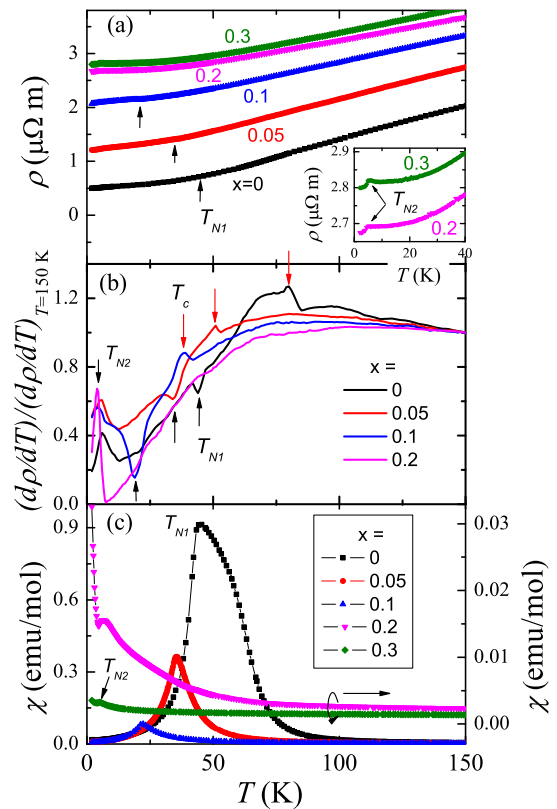


FIG. 6. (a) Temperature dependence of resistivity (ρ) for the $\text{SmCo}_{1-x}\text{Fe}_x\text{AsO}$ ($x = 0, 0.05, 0.1, 0.2, 0.3$) samples. (b) The derivative of resistivity below 150 K. The data are normalized to $(d\rho/dT)_{T=150\text{K}}$. (c) Temperature dependence of magnetic susceptibility (χ) under a magnetic field of 1000 Oe in the zero-field-cooled (ZFC) configuration. The inset shows the enlarged resistivity for $x=0.2$ and 0.3 at low temperature.

in previous works^{18,20}, SmCoAsO undergoes three magnetic phase transitions at T_c , T_{N1} , and T_{N2} , respectively. The magnetization sharply increases and saturates with increasing field between T_c and T_{N1} . In order to study the magnetic structure at different temperatures, these data are collected at temperature where PM or FM state dominates in Fig. 6(b), and 2 K. Obviously, for $x \leq 0.1$, the $M - H$ curve is linear at 2 K and above T_c , and the "S" shape of FM behavior is only observed between T_c and T_{N1} . As x increases to 0.2, the linear feature is observed only above T_c , and the M-H curve displays FM behavior below 2 K, implying that the AFM transition T_{N1} approaches to zero. This feature is different from the case of $\text{NdCo}_{1-x}\text{Fe}_x\text{AsO}^{27}$, where both FM and AFM order are not observed around 0.2. At $x = 0.3$, the M-H curves goes back to the linear behavior at 2 K, indicating that the FM order from the Co sublattice is completely destroyed. On the other hand, with increasing Fe content, both the saturation moment and the transition

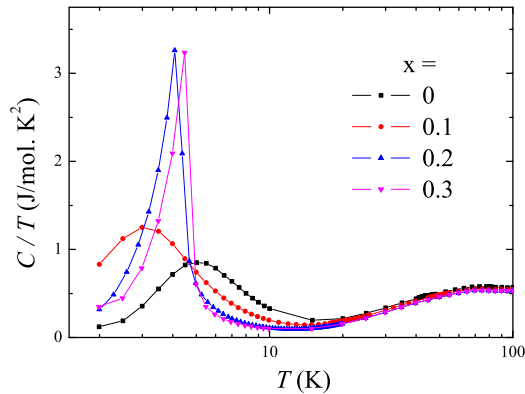


FIG. 7. The specific heat of $\text{SmCo}_{1-x}\text{Fe}_x\text{AsO}$ ($x = 0, 0.05, 0.1, 0.2, 0.3$) samples under at zero field below 100 K.

temperature (T_c) gradually decrease, implying that the 3d-electron magnetism becomes weaker.

Based on above data, the magnetic phase diagram of $\text{LnCo}_{1-x}\text{Fe}_x\text{AsO}$ is established in Fig. 9. In $\text{LaCo}_{1-x}\text{Fe}_x\text{AsO}$, the T_c associated with FM transition is sharply suppressed and disappears around $x = 0.3$. At the same time, in the $\text{SmCo}_{1-x}\text{Fe}_x\text{AsO}$ system, the T_{N1} from FM to AFM transition of Co sublattice is shifted to lower temperatures with increasing Fe content and such transition has not been observed at $x = 0.2$. Meanwhile the T_c , the FM order gradually decreases and is completely suppressed at $x = 0.3$, similar to the case of $\text{LaCo}_{1-x}\text{Fe}_x\text{AsO}$. Here, we note that for the Co-parent compounds T_c increases slightly when La is replaced by Sm. But a new FM-AFM transition of the 3d-electrons is induced in the later case. This manifests an interesting interplay between the 3d-electrons and the local Sm^{3+} moments.

Thus, in the 1111-type Co-based $\text{LnCo}_{1-x}\text{Fe}_x\text{AsO}$ systems, 4f electrons of rare earth elements have an important effect on the magnetic behavior of 3d electrons. Whereas, the antiferromagnetic transition temperature of Sm moments T_{N2} almost does not change within the whole doping regime. It implies that the AFM ordering of the Sm 4f-electrons is robust against Fe/Co substitution within the CoAs layer. Therefore, the microscopic origin of the f-electron AFM order of this system should be mainly due to the superexchange interactions between the f-local moments²⁸. These superexchange interactions are bridged by two kinds of f-p orbital hybridizations: one via Sm-O path and another the Sm-As path, respectively²⁸. Meanwhile, the RKKY interaction mediated by the charge carriers within the CoAs layer may not play a crucial role for the f-electron magnetism because the RKKY interaction would be explicitly dependent on the variations of 3d-electrons. Because the radius of Sm^{3+} ion is smaller than La^{3+} , one may spec-

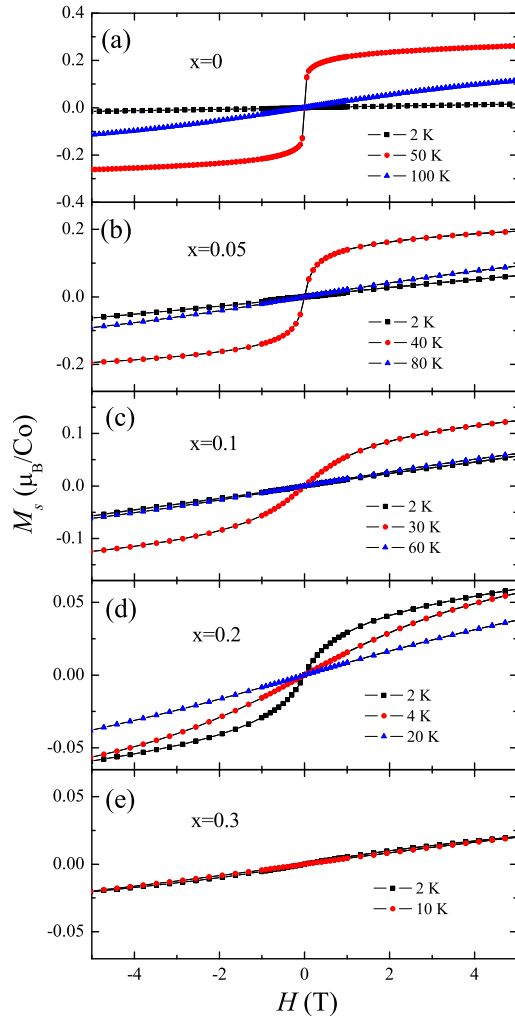


FIG. 8. Magnetic field dependence of magnetization at several different temperature for the $\text{SmCo}_{1-x}\text{Fe}_x\text{AsO}$ ($x = 0, 0.05, 0.1, 0.2, 0.3$) samples.

ulate that the FM-AFM transition is not related to the magnetic 4f-electrons, but rather due to the enhancement of three dimensionality as the lattice parameter c decreases. In order to clarify this possibility, we have also performed LDA calculations on LaCoAsO but using the lattice parameters of SmCoAsO . We do find that the FM state of Co d-electrons is robust against the decreasing lattice constant. Experimentally, Similar results were always observed in NdCoAsO under pressure²⁹. Therefore, we suggest that the FM-AFM transition at T_{N1} of the 3d-electrons should be due to their coupling (polarization) to the 4f-moments along the z -direction.

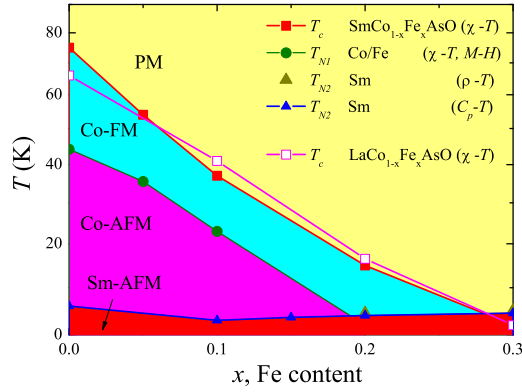


FIG. 9. Magnetic phase diagram for the $\text{SmCo}_{1-x}\text{Fe}_x\text{AsO}$ (solid) and $\text{LaCo}_{1-x}\text{Fe}_x\text{AsO}$ (open) system, respectively. The transition temperatures were determined from the measurements of magnetic susceptibility, magnetization and specific heat. T_{N2} is taken from resistivity and specific heat data.

IV. CONCLUSION

In the 1111 Co-based $\text{LnCo}_{1-x}\text{Fe}_x\text{AsO}$ ($\text{Ln}=\text{La}, \text{Sm}$) system, a series of $\text{LnCo}_{1-x}\text{Fe}_x\text{AsO}$ samples have been

synthesized, and their transport and magnetic properties were investigated. A rich magnetic phase diagram of the $\text{LnCo}_{1-x}\text{Fe}_x\text{AsO}$ systems is then established. The FM order is observed in both LnCoAsO ($\text{Ln} = \text{La}, \text{Sm}$) systems, and is completely destroyed with increasing Fe doping content to 0.3. Meanwhile, in $\text{SmCo}_{1-x}\text{Fe}_x\text{AsO}$, T_{N1} is suppressed to below 2 K as $x = 0.2$, but the AFM order of rare earth element Sm ion survives in the whole doping regime $x \leq 0.3$. This also indicates that the disorder effect induced by Fe/Co doping is very weak. Based on these results, it is concluded that in $\text{LnCo}_{1-x}\text{Fe}_x\text{AsO}$ systems, while the magnetic properties of the 4f electrons of rare earth elements are robust against the variations of 3d electrons, they do play a significant role in the magnetic behaviors of the 3d electrons. These materials therefore provide a prototypical testing ground for exploring the interplay between 4f and 3d electrons in transition metal compounds.

ACKNOWLEDGMENTS

Y.K. Li would like to thank J. H. Dai for discussions. This work is supported by the National Basic Research Program of China (Grant No. 2011CBA00103), NSFC (Grant No. 11174247, and 11104053), and the National Science Foundation of Zhejiang Province (Grant No. Z6110033, and R12A040007).

- ¹ Y. Kamihara, T. Watanabe, M. Hirano, and H. Hosono, *J. Am. Chem. Soc.* **130**, 3296 (2008).
- ² H. Yanagi, R. Kawamura, T. Kamiya, Y. Kamihara, M. Hirano, T. Nakamura, H. Osawa, and H. Hosono, *Phys. Rev. B* **77**, 224431 (2008).
- ³ H. Ohta and K. Yoshimura, *Phys. Rev. B* **79**, 184407 (2009)
- ⁴ H. Ohta, C. Michioka, and K. Yoshimura, *Phys. Rev. B* **84**, 134411 (2011).
- ⁵ C. de la Cruz, Q. Huang, J. W. Lynn, J. Li, W. Ratcliff II, H. A. Mook, G. F. Chen, J. L. Luo, N. L. Wang, and P. C. Dai, *Nature* **453**, 899 (2008).
- ⁶ M. Rotter, M. Tegel, and D. Johrendt, I. Schellenberg, W. Hermes, and R. Pttgen, *Phys. Rev. B* **78**, 020503(R) (2008).
- ⁷ K. Kayanuma, H. Hiramatsu, T. Kamiya, M. Hirano, and H. Hosono, *J. Appl. Phys.* **105**, 073903 (2009).
- ⁸ Z. Li, G. Chen, J. Dong, G. Li, W. Hu, D. Wu, S. Su, P. Zheng, T. Xiang, N. Wang, and J. Luo, *Phys. Rev. B* **78**, 060504(R) (2008).
- ⁹ H. Ohta, K. Yoshimura, *Phys. Rev. B* **80**, 184409, (2009).
- ¹⁰ A. S. Sefat, A. Huq, M. A. McGuire, R. Y. Jin, B. C. Sales, D. Mandrus, L. M. D. Cranswick, P. W. Stephens, and K. H. Stone, *Phys. Rev. B* **78**, 104505 (2008).
- ¹¹ C. Wang, Y. K. Li, Z. W. Zhu, S. Jiang, X. Lin, Y. K. Luo, S. Chi, L. J. Li, Z. Ren, M. He, H. Chen, Y. T. Wang, Q. Tao, G. H. Cao, and Z. A. Xu, *Phys. Rev. B* **79**, 054521 (2009).
- ¹² J. Prakash, S. J. Singh, S. Patnaik, and A. K. Ganguli, *Solid State Commun.* **149**, 181 (2009).
- ¹³ X. Lin, H. J. Guo, C. Y. Shen, Y. K. Luo, Q. Tao, G. H. Cao, and Z. A. Xu, *Phys. Rev. B* **83**, 014503 (2011).
- ¹⁴ P. Shirage, K. Miyazawa, H. Kito, H. Eisaki, and A. Iyo, *Physica C* **469**, 898 (2009).
- ¹⁵ A. Marcinkova, D. A. M. Grist, I. Margiolaki, T. C. Hansen, S. Margadonna, and J. G. Bos, *Phys. Rev. B* **81**, 064511 (2010)
- ¹⁶ H. Ohta, C. Michioka, and K. Yoshimura, *J. Phys. Soc. Jpn.* **79**, 054703 (2010).
- ¹⁷ M. A. McGuire, D. J. Gout, V. O. Garlea, A. S. Sefat, B. C. Sales, and D. Mandrus, *Phys. Rev. B* **81**, 104405 (2010).
- ¹⁸ V. P. S. Awana, I. Nowik, P. Anand, K. Yamaura, M. E. Takayama, and I. Felner, *Phys. Rev. B* **81**, 212501 (2010).
- ¹⁹ H. Ohta, C. Michioka, A. Matsuo, K. Kindo, and K. Yoshimura, *Phys. Rev. B* **82**, 054421 (2010).
- ²⁰ Y. K. Li, Tong J, Han H, Zang L, Tao Q, Cao G H, Xu Z A, *Science China* **53**, 1194 (2010).
- ²¹ J. Sugiyama, M. Mnsson, O. Ofer, K. Kamazawa, M. Harada, D. Andreica, A. Amato, J. H. Brewer, E. J. Ansaldo, H. Ohta, C. Michioka, and K. Yoshimura, *Phys. Rev. B* **84**, 184421 (2011)
- ²² A. Pal, M. Tropeana, S. D. Kaushik, M. Hussain, H. Kishan, and V. P. S. Awana, *J. Appl. Phys.* **109**, 07E121 (2011).
- ²³ A. Pal, S. S. Mehdi, M. Husain, B. Gahtori, and V. P. S. Awana, *J. Appl. Phys.* **110**, 103913 (2011).

- ²⁴ S. Riggs, C. Tarantini, J. Jaroszynski, A. Gurevich, A. Palenzona and M. Putti, T. Duc Nguyen and M. Affronte, Phys. Rev. B **80**, 214404 (2009)
- ²⁵ J. Sugiyama, M. Mnsson, O. Ofer, K. Kamazawa, M. Harada, D. Andreica, A. Amato, J. H. Brewer, E. J. Ansaldo, H. Ohta, C. Michioka, and K. Yoshimura, Phys Rev B **84**, 184421, (2011).
- ²⁶ J. P. Perdew, K. Burke, M. Enzerhoff, Phys. Rev. Lett **77**, 3865 (1996).
- ²⁷ Michael A. McGuire, Athena S. Sefat, Brian C. Sales, and David Mandrus, Phys. Rev. B **82**, 092404 (2010).
- ²⁸ J. Dai, J.-X. Zhu, and Q. Si, Phys. Rev. B. **80**, 020505 (2009).
- ²⁹ W. Uhoya, G. MTsoi, Y. K. Vohra, M. A McGuire, A. S. Sefat, B. C. Sales, D. Mandrus and S. T. Weir, J. Phys.: Condens. Matt. **22**, 185702 (2010).